NASA Technical Memorandum 81386

COMPARISON OF INLET SUPPRESSOR DATA WITH APPROXIMATE THEORY BASED ON CUTOFF RATIO

Edward J. Rice and Laurence J. Heidelberg
Lewis Research Center
Cleveland, Ohio

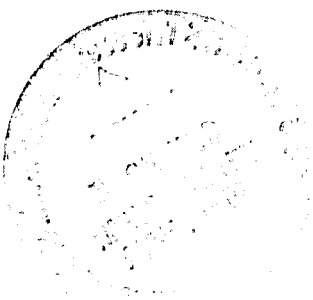

Prepared for the
Eighteenth Aerospace Sciences Meeting
sponsored by the American Institute of
Aeronautics and Astronautics
Pasadena, California, January 14-16, 1980

COMPARISON OF INLET SUPPRESSOR DATA WITH APPROXIMATE THEORY BASED ON CUTOFF RATIO

by

Edward J. Rice* and Laurence J. Heidelberg+
NASA Lewis Research Center
21000 Brookpark Road
Cleveland, Ohio 44135

ABSTRACT

This paper represents the initial quantitative comparison of inlet suppressor far-field directivity suppression with that predicted using an approximate liner design and evaluation method based upon mode cutoff ratio. The experimental data was obtained using a series of cylindrical point-reacting inlet liners on an Avco-Lycoming YF102 engine. The theoretical prediction program is based upon simplified sound propagation concepts derived from exact calculations. These indicate that all of the controlling phenomenon can be approximately correlated with mode cutoff ratio which itself is intimately related to the angles of propagation within the duct. The objective of the theory-data comparisons is to point out possible deficiencies in the approximate theory which may be corrected. After all theoretical refinements have been made, then empirical corrections can be applied.

E-294

INTRODUCTION

There is a need for an accurate but simplified method for designing and evaluating suppressors without splitters for aircraft engine inlets. Methods have been published[1,2] which can be used to estimate acoustic power reduction in exhaust ducts or in inlets with splitter rings. However, what is really needed is a comprehensive, generally available, design or evaluation program which provides acoustic suppression information in the far-field.

Comprehensive suppressor evaluation is a very complex problem involving source acoustic power description, suppressor effectiveness, modal scattering at several places in the propagation path and, finally, radiation to the far-field. The complete coupled system may never be amenable to analysis, except perhaps by some as yet undeveloped numerical analysis program. The method used in this paper represents a first order, uncoupled, analytical approach to each element of the propagation and radiation problem. Each element was found to be dependent upon the mode cutoff ratio, which provides a great simplification to the entire problem. This dependence upon cutoff ratio has been reported for maximum possible attenuation[3], optimum impedance[4], duct termination reflection[5], far-field radiation directivity[5] and modal density function[6].

The purpose of this paper is to compare calculated noise suppression results using the simplified analysis, in its present state of development, with experimental inlet suppressor data reported in reference 7. The comparison will be made on the basis of far-field attenuation directivity. This comparison, made on an angle-by-angle basis, is extremely demanding since it encompasses all elements of the problem starting with the description of the noise source and then proceeding with the suppressor performance and, finally, the sound radiation from the duct inlet. The far-field attenuation directivity is, however, the essential information needed for suppressor performance.

*Head, Acoustics Section; Member AIAA
+Aerospace Engineer; Member AIAA

The future work concerning this simplified liner evaluation approach will proceed in two directions. The theory-data comparisons will be used to point out where further analytical effort is required to encompass more of the essential physics into the program. Also, an effort will be made to account for missing phenomena by empirical corrections to the theory.

SYMBOLS

B1, B2, B3	three inlet liner constructions (Table i)
BPF	blade passage frequency, Hz
b	liner backing depth, m
c	speed of sound, m/sec
$\mathcal{D}$	modal density function, see equation (7)
D	circular duct diameter, m
d_o	orifice diameter in perforated plate, m
ΔdB	sound attenuation, decibels
ΔdB_m	maximum possible sound power attenuation, decibels
ΔdB_3	sound attenuation using liner B3 only, decibels
ΔdB_{32}	sound attenuation using both liners B3 and B2, decibels
ΔdB_{321}	sound attenuation using liners B3, B2 and B1, decibels
F	quantity in circular contour correlation, see equation (A5)
f	frequency, Hz
I_{INC}	acoustic intensity incident upon duct termination, N/MS
I_T	acoustic intensity transmitted out from termination, N/MS
L	length of acoustic treatment, m
M_D	axial steady flow Mach number, free-stream uniform value

m	spinning mode lobe number (circumferential order)
N	number of modes
n	exponent in cutoff ratio biasing function, see equations (6) and (8)
P	far-field acoustic pressure amplitude, N/M^2
P_m	far-field acoustic pressure amplitude due to multiple modes, N/M^2
R	eigenvalue for circular hardwalled duct or absolute value of complex eigenvalue for softwall duct
$\mathcal{R}$	radius in circular damping contour correlation, see equation (A4)
r_o	circular duct radius, m
t	perforated plate thickness, m
Ul	inlet liner (Table I)
α	radial eigenvalue
β	cutoff ratio biasing function, see equation (8)
γ	$\Delta dB_m/\Delta dB$
δ	1/7th power boundary layer thickness, m
δ^*	displacement boundary layer thickness, m
ε	δ/r_o
η	frequency parameter, $\eta = fD/C$
Θ	specific acoustic resistance
θ_c	resistance coordinate for center of damping contour
θ_m	optimum specific acoustic resistance
θ_{mo}	optimum specific acoustic resistance without boundary layer (slip flow)

μ	radial mode order index
ξ	mode cutoff ratio
σ	liner open area ratio
ϕ	phase of complex eigenvalue, degrees
χ	specific acoustic reactance
χ_c	reactance coordinate for center of damping contour
χ_m	optimum specific acoustic reactance
ψ	far-field angle measured from inlet duct axis, degrees
ψ_p	ψ at peak of principal lobe of radiation
ψ_o	directivity angle without flow, degrees

SIMPLIFIED APPROXIMATE SUPPRESSOR THEORY

In this section the elements of the simplified suppressor theory will be outlined. Since this paper represents an initial theory-data comparison and not a final recommended procedure, many of the correlations used will be only referenced. Only the recent changes in the procedure and expressions which are useful in later discussions will be listed explicitly. The subjects covered include suppressor performance, far-field radiation and duct termination effects, source power distribution and assumptions implicit in using the above as uncoupled elements in a system which is actually coupled.

Suppressor Performance

The sound attenuation obtained in a cylindrical suppressor is obtained by using correlations of the optimum impedance and maximum possible attenuation. These feed into a circular approximation correlation of the actual damping contours which are used to estimate off-optimum suppressor performance.

The concepts of optimum impedance and maximum possible attenuation are illustrated in Figure 1. Equal damping contours representing exact calculations for a particular mode ($m = 7$, $\mu = 1$) are represented by the solid lines. As damping is increased, the contours shrink in size and the limit is represented by the optimum impedance. The damping at this limiting

impedance is called the maximum possible attenuation for this mode. Pushing to higher attenuations would result in a contour which can be related to the next higher radial mode ($\mu = 2$ in this case). In reference 8 it was discovered that modes with similar cutoff ratios had similar optimum impedances. This idea was pursued in reference 4, in which a wide range of parametric study of optimum impedance was made. The mode cutoff ratio defined in the suppressor section as,

$$\xi = \frac{\pi\eta}{R\sqrt{(1-M_D^2)\cos 2\phi}} \tag{1}$$

was found to correlate the optimum impedance quite accurately. The only modal information required is, thus, the cutoff ratio. The optimum impedance components are found using the procedure reported in reference 4 and are a function of the frequency parameter (η), boundary layer thickness, steady flow Mach number and, of course, cutoff ratio.

The maximum possible attenuation was also shown to be approximately correlated by cutoff ratio alone[3]. The expression used here is,

$$\frac{\Delta dB_m}{L/D} \approx \frac{327\,\xi}{1-M_D^2}\left\{\frac{0.9221}{\xi^2} - 1 + \sqrt{1 - \frac{1.8442}{\xi^2} + \frac{0.879}{\xi^4}}\right\}^{1/2} \tag{2}$$

Equation (2) shows that maximum possible attenuation is a function only of cutoff ratio, Mach number and duct L/D. Although optimum impedance can be a strong function of boundary layer thickness[4,9], it was shown in reference 9 that the maximum damping is insensitive to boundary layer thickness.

Off-optimum suppressor performance is evaluated by an approximate circular damping contour correlation similar to that developed in reference 10. This approximate correlation is compared to exact calculations in Figure 1 for a well propagating mode (large ξ). The correlation of reference 10 was semi-empirical and was based upon calculations made for well propagating modes. When theory-data comparisons of far-field radiation attenuation were made, it became obvious that the circular contours were not sufficiently broad for cutoff ratios near unity. An evaluation of the exact equal damping contours near cutoff was made and the correlation was altered to reflect this near cutoff broadening. The new correlation is presented in the Appendix. An additional change from the correlation of reference 10 is also found in the Appendix. When optimum resistance is reduced due to boundary layer refraction, the entire family of contours is also compressed. The new correlation is compared to exact attenuation contours for a near cutoff mode in Figure 2. Notice that for low attenuation (larger contours) the contours do not close as they did in Figure 1 for high cutoff ratio.

Far-Field Radiation

The basis of the far-field radiation expression used for the calculation reported here is[5],

$$p^2 \approx \frac{2 \sin\psi \sqrt{1-1/\xi^2} \left\{\sin[\pi\eta(\sin\psi - 1/\xi)]\right\}^2}{\pi^2\eta \left[1/\xi^2 - \sin^2\psi\right]^2} \tag{3}$$

which has the principle lobe peak located approximately at the angle given by,

$$\sin\psi_p \approx 1/\xi \tag{4}$$

where the mode cutoff ratio (ξ) is defined by,

$$\xi = \frac{\pi\eta}{R} \tag{5}$$

Equation (3) represents an approximation to the exact equation for a flanged duct with equal acoustic power per mode[11]. The modification to the exact expression to yield equation (3) was made mainly to allow the expression to be only a function of cutoff ratio (ξ) by the suppression of modal information (m, α). The approximations involve using the sinusoidal approximation to the Bessel function and assuming that $m/\alpha << 1$. Equation (3) represents an adequate approximation to the exact flanged duct expression except for the lower radials of the high lobed (larger m) modes where some error occurs[12].

The far-field radiation pattern for multimodal radiation can be approximated by,

$$p_m^2 \approx 2 \cos\psi \sin^n\psi \tag{6}$$

which was derived in reference 5 by consideration of the amplitude and location of the principal lobe of equation (3) and using the modal density function[6]

$$\mathscr{D} = \frac{1}{N}\frac{dN}{d\xi} \approx \frac{2}{\xi^3} \tag{7}$$

and the cutoff ratio biasing function[5],

$$\beta \approx 1/\xi^n \tag{8}$$

Equation (6) expresses the effect of the summation of all of the principal lobes of radiation for the propagating modes. Equation (7) allows the estimation of the relative number of modes within a desired cutoff ratio range, and equation (8) allows the biasing of the source distribution towards cutoff away from equal acoustic power per mode. Note that when $n = 0$ equal acoustic power per mode is used and equation (6) reduces to the simple expression $2 \cos \psi$. Exact summations, using the flanged duct radiation equation, of all the propagating modes were made for $n = 0$, 1, 2 and 3 in reference 12. Equation (6) was shown to be an extremely good approximation.

In a static test case for an engine inlet, where there is no flow in the far-field, it was found that the far-field radiation is shifted toward the inlet axis. The position of the peak of the principal lobe of radiation was found to be given by[13],

$$\cos \psi_p \approx \frac{-M_D + \sqrt{1-1/\xi^2}}{1 - M_D\sqrt{1-1/\xi^2}} \tag{9}$$

where now the cutoff ratio must be defined by,

$$\xi = \frac{\pi \eta}{R\sqrt{1-M_D^2}} \tag{10}$$

This radiation direction shift is caused by the change in axial propagation angle for a duct mode due to the convective velocity effect[13]. An example of this effect is that at $M_D = -0.4$, a mode near cutoff ($\xi \approx 1$) propagates at 66^o from the inlet axis. At $M_D = 0$, a near cutoff mode has its peak propagation at 90^o. This idea was further generalized in reference 14 to include the entire radiation pattern. The corrected radiation directivity including the convective effect can be expressed as,

$$\cos \psi = \frac{-M_D + \sqrt{1 - (1-M_D^2)\sin^2 \psi_o}}{1 - M_D\sqrt{1 - (1-M_D^2)\sin^2 \psi_o}} \tag{11}$$

where ψ_0 is the directivity angle without flow. This directivity shift toward the inlet axis was found to be essential to explain the experimental attenuation data. Unfortunately, this shift was made only in the final attenuation calculations and has not yet been integrated into the computer program. For example, equation (6) must be altered by the convective shift to accommodate the principle lobes of radiation, and the shift must be applied also to the side lobes of equation (3) (see reference 5 for current handling of side lobes). It is expected that the integration of the convective directivity shift will not greatly alter the results presented in this paper; however, this has not been checked.

One problem occurs when the convective radiation shift is applied. Since the flanged duct radiation theory applies only to 90° for a no-flow situation, after the shift toward the inlet axis is made the theory will only extend to about 66° (see example above). Thus, an unflanged radiation directivity expression is needed for this program. These results are available in the literature[15, 16, 17], however, they are too unwieldy for routine use in a multimodal radiation calculation. More significantly, these equations have not yet been reduced to a form containing modal information only in the form of cutoff ratio so that they can be integrated into the current program. Effort is underway to obtain a simple, adequate approximation for this purpose.

A duct termination loss is also used in this program. This termination effect was derived in reference 5 and is given by,

$$\frac{I_T}{I_{INC}} \approx \frac{4\sqrt{1-1/\xi^2}}{\left(1+\sqrt{1-1/\xi^2}\right)^2} \tag{12}$$

Equation (12) contains only the mode cutoff ratio. It is known to the author that a better expression containing also the frequency parameter (η) should be used, but is has not been completed at this time.

Source Power Distribution

It is known that the sound power attenuation provided by an acoustic liner is strongly dependent upon the acoustic mode present in the liner[1,18]. Likewise, with a multitude of modes present, the attenuation should be a function of the distribution of acoustic power among the modes. The method presented in this paper does not use modes directly, but instead bases all of the elements of the program upon mode cutoff ratio. Thus, modal power distribution is replaced by cutoff ratio power distribution. This is an important simplification since although many modes may be present within a small increment of cutoff ratio, it is not necessary to know the power of the individual modes but only the total power of all of these modes.

This simplification also has practical significance. Although experimental measurement of modal amplitude and phase has been attempted for quite simple modal structures in rectangular[19] and annular[20] ducts, it appears that if a large number of modes is possible then direct modal measurement will be extremely difficult[20], if not impossible.

The only available method to estimate an acoustic power distribution is to observe the far-field directivity pattern and to infer the source distribution which could have caused this radiation pattern as in references 5 and 11. This indirect method is usable for a single mode or for multimodal propagation where the modes are uncorrelated. It would be difficult to assess the radiation pattern of a few correlated modes but then, of course, direct modal measurement in the duct would be feasible. Equation (6) can be used for a comparison with the far-field experimental directivity data and the exponent n can then be estimated. Equation (8) will then show the biasing away from equal energy per mode. This was done in reference 7 for the fan blade passage tone considered in this paper with the result that $n \approx 0$. Another method that could be used when the principal lobes of radiation dominate the entire directivity pattern is to compare directivity data at each angle to equation (6). Since the far-field directivity would be dominated by radiation from modes of a particular cutoff ratio range, then several discrete corrections (away from equal power per mode) at several cutoff ratios could be obtained. This refinement was not attempted here due to the previously mentioned corrections which have yet to be developed for equation (6) to account for duct flow convective directivity shift. Thus, as a first approximation, equal acoustic power per mode ($n = 0$) will be used for all of the calculations presented in this paper.

Inherent Assumptions of Present Program

Several intrinsic assumptions are embodied in the methods as presently reported. First, it is assumed when many modes are present and that they are uncorrelated so the squares of the pressures (as in eq. (3)) can be summed (the squares of the sum of pressures must be used for correlated modes). This is probably valid for randomly generated noise such as broadband noise or even tones generated by inflow turbulence.

Second, it is assumed that for a multitude of modes at all possible cutoff ratios, modal scattering has no net effect. For a single mode, the scattering occurring between a hard-walled and treated section could certainly affect the calculated suppression. Different radial boundary conditions are present between the hard- and soft-walled sections. Thus, differing axial and radial propagation angles will occur between the two

sections (see reference 21 for discussion of propagation angles in lined ducts). Therefore, although there is no circumferential scattering, due to circumferential symmetry, there will, in general, be radial mode scattering occurring. This radial scattering is probably a function of cutoff ratio, frequency parameter, Mach number and wall impedance. Although scattering is known to occur, to simplify the problem it is assumed that the scattering will balance out. For example, a given acoustic power versus cutoff ratio distribution may exist in the hard duct. For each group of modes near a given cutoff ratio there will be scattering to both higher and lower cutoff ratios. It is assumed that as much power is received from other cutoff ratio modes as is lost to them. Thus, the power distribution in the soft duct (based upon cutoff ratio) is the same as that in the preceding hard duct. A study of this phenomena must yet be made, and it is possible that some of the discrepancies between theory and data, which are discussed in a later section, are due to neglect of this phenomenon.

Reflections at impedance and area discontinuities are ignored except for the crude duct termination effect given by equation (12). This equation is an approximation for the reflection of a given mode with the same mode incident. Actually, there will be some radial mode scattering and reflection (similar to that discussed above in connection with the hard-soft wall interface). Subtle radiation pattern changes may occur which would lead to disagreement between theory and data. However, this effect is judged to be of less importance than that at the hard-soft interface.

It is also assumed that the inlet lip shape has no effect upon the far-field radiation pattern. This effect is probably small for inlets with fairly abrupt lips and with high Mach number. The high Mach number causes the modal wave fronts to propagate at small to moderate angles to the axis[13] (only up to 66° for $M_D = -0.4$) and, put very simply, the emerging wave does not see an abrupt change in the lip. A gradual area change is quite another case; the decreasing Mach number and increasing radius can affect the propagation angles and, thus, the radiation angle. These effects are currently being studied and will be incorporated into the program when available.

PROCEDURE FOR CALCULATING THEORETICAL ATTENUATION

The procedure for combining the theoretical elements discussed in the previous sections will now be outlined. Figure 3 will be used to help illustrate the calculation of the far-field directivity attenuation. The calculations are made for a particular frequency, duct Mach number, boundary layer thickness and duct geometry. The optimum impedance locus (the solid curve) is first generated by either exact

modal calculations or more conveniently using the correlation equations in terms of cutoff ratio from reference 4. The locations of the centers of equal mode number intervals are found[3] using the modal density function, equation (7). Five of these locations are shown for illustration in Figure 3 but many more are used in the calculations shown later in this paper. Note that each of these points has a cutoff ratio associated with it and a preferred radiation direction is noted for each as calculated from equation (4). Plots of the experimental hard-wall far-field directivity are compared to equation (6) to get an estimate of the acoustic power distribution. Note that unless a bias (eq. (8)) is applied, all points on the locus of Figure 3 will contain equal acoustic power since they contain an equal number of modes.

Each of the modal groups is used to form a hard-wall far-field radiation pattern using the flanged duct equations of reference (5). This represents a simplified integration process over all modes whose principle lobes of radiation can contribute to a particular far-field angle. The procedure is the same as that used to derive equation (6). Sidelobes are also considered. The sidelobes of modes at all cutoff ratios can possibly contribute to the radiation at any given angle in the far-field. An integration procedure is also used for the sidelobes as presented in reference 5. The hard-wall far-field radiation pattern is, thus, established at the five angles represented in Figure 3.

For the lined duct configuration, a wall impedance of interest (or an actual wall impedance for a particular liner) is chosen as in Figure 3. The damping of each of the five modal groups must then be calculated. The maximum possible attenuation is calculated using equation (2) and, of course, the optimum impedance is already known (the point on the locus). Off-optimum attenuation (the circles and the rectangular point in Figure 3 do not generally coincide) is then calculated using the equations in the Appendix (illustrated in Figures 1 and 2) defining the approximate circular damping contours. The original acoustic power at each cutoff ratio is, thus, reduced by a certain amount by the liner and this reduced acoustic power is radiated to the far-field as in the hard-wall case. The difference between the hard-wall and soft-wall far-field directivities thus represents the far-field directivity attenuation. Equation (11) is then used to shift the directivity attenuations from the original angles ψ_o to corrected angles ψ. This accounts for the convective effect present with flow in the inlet duct and no flow in the far-field (i.e., the static test case).

The above discussion using five mode groups and, thus, five far-field angles was used for illustration only. The actual program uses 40 different cutoff ratios to establish the function of suppression versus cutoff ratio. Interpolation is then used as needed. Far-field radiation patterns are calculated every 5 degrees from 5 degrees to 85 degrees. The convective correction (equation (11)) must be applied to each of these angles.

DATA-THEORY COMPARISONS

The data reported here were obtained using six inlet suppressors used singly and together on an Avco-Lycoming YF102 engine. The engine was run with a large aft muffler which removed all aft fan, core, and jet noise and assured that only inlet noise was being studied. Each liner section had a length to diameter ratio of one-half. The data reported here was for the fan blade passage frequency. Additional details concerning the tests and the liner construction can be found in reference 7, which also contains a large amount of additional data. The parameters for the liners for which data is reported here are found in Table I. The resistance and reactance were calculated using[7]

$$\Theta = \frac{M_D}{\sigma(2 + 1.256\ \delta^*/d_o)} \tag{13}$$

$$\chi = \frac{2\pi ft}{\sigma c} - \cot \frac{2\pi fb}{c} \tag{14}$$

The loci of optimum impedance for the highest speed engine conditions for three boundary layer thicknesses, as well as the impedances of the six liners, are shown in Figure 4. These calculations, as well as all that follow, are for the blade passage frequency of 4734 Hz. Three boundary layer thicknesses were considered in Figure 4 to represent an average value for each of the liner locations. Liner B1, being located nearest the inlet lip, is associated with the thinnest boundary layer while liner B3, nearest the fan, is located in the thickest boundary layer region. All possible propagating modes were considered in generating the optimum impedance loci. Mainly axial or well propagating modes with high cutoff ratio are located on the left end of the loci while near cutoff ($\xi \approx 1$) or mainly transverse propagating modes are located at the bottom right. As can be seen, liner B3 was designed for near cutoff modes, B2 for intermediate cutoff ratios, and B1 for well propagating modes. All of the liners were intended to fall on the loci, but due to a deficiency in the earlier impedance model used at the time of the design, the liners are all under-damped as compared to the target values. This will not affect the comparisons shown here. Liner B3 was anticipated to provide the highest attenuation, located mostly to the sideline due to the damping and radiation properties of near cutoff modes. Liner B2 should provide more modest attenuation somewhat nearer to the inlet centerline. Liner B1 should have lower attenuation located even more toward the centerline. The above is based upon single mode reasoning. With a multitude of modes there is a complicated superposition of radiation patterns, and modes at different cutoff ratios will all be

attenuated differently. Hence, the real situation will be much more complicated than described above. However, if the data is properly taken and interpreted, the above qualitative liner behavior can be seen.

Liners B4 and B5 were included to provide underdamped and overdamped versions of liner B3. The variation of far-field directivity attenuation with liner resistance can be studied using these three liners. Two sections of liner U1 were built to represent somewhat of a baseline, since this liner represented our best estimate of a good uniform liner at the time the liners were designed.

Figure 5 shows the experimental results and the theoretical comparisons for a progressive untaping of the B1, B2, B3 liners. At first, all of the liners are taped to establish a hard-wall baseline and to estimate the acoustic power versus cutoff ratio distribution as discussed in the previous section. When liner B3 is untaped (located nearest the fan), the directivity attenuation shown by the circle symbols is obtained. The peak attenuation occurs somewhat less than $\psi = 70$ degrees and is quite large (about 9 dB). The angle shift due to convective effects in the duct inlet, as represented by equation (11), is seen to be essential to obtain even qualitative agreement between theory and data. Without this shift, the theoretical curve for liner B3 would have peaked at $\psi = 90$ degrees. This would occur since there are many modes near cutoff which are easily damped, and according to the zero Mach number flanged duct theory, these would radiate near 90 degrees from the inlet axis.

With this convective correction as applied in Figure 5 the theoretical attenuation directivity agrees quite well with the data. There is an overprediction of about 35 percent at the peaks, which is quite good for this initial comparison. The second set of data, labeled $B_{32} - B_3$, is obtained by subtracting the attenuation of liner B3 only from that when both B3 and B2 are untaped. Thus, liner B2 is working on the modes emerging from liner B3, which should be deficient in modes near cutoff. Again, the agreement with the theory is quite good. The final set of data, labeled $B_{321} - B_{32}$, is again an incremental attenuation due to liner B1 operating on the modes remaining after attenuation by liners B3 and B2. Near cutoff and moderately cutoff modes should be deficient, leaving only axially or well propagating modes. The remaining attenuation is quite small and is seen to be accurately predicted by the theory. The abrupt termination in the theoretical curves at about 62 degrees is due to the use of the flanged duct radiation model. This model is valid only to 90 degrees for zero Mach number and this point is shifted down to near 60 degrees due to the convective correction discussed above. Use of an unflanged radiation model will alleviate this problem.

Although the predictions are a little larger than the data in Figure 5, the qualitative description is excellent. It should be noted that no corrections have yet been applied for inactive liner area due to fastening of the liner perforate to the spool piece flanges. After this has been accounted for, a simple empirical correction could be applied to provide excellent agreement near the peak. This has not yet been done since there are first order changes which must yet be made to the approximate theory. This will become more apparent in the later discussions. No explanation can be made at this time as to why the theory is inconsistent at small angles.

In Figure 5 liner B3 was tested in isolation but liners B2 and B1 were tested with a somewhat conditioned power input distribution. That is, other liners had operated upon the power distribution before it entered B2 or B1. Data from tests of liners B2 and B1 by themselves are shown in Figure 6. The directivity attenuations are quite different than for the tests shown in Figure 5. This is true in particular for liner B1 shown in Figure 6 (compare to lowest data points in Figure 5). Under the test conditions shown in Figure 5, liner B1 had only the well propagating modes to operate upon, but when tested in isolation the full range of power for all cutoff ratios was available. The attenuation is much larger in Figure 6 and is biased toward larger angles. This is due to the presence of near cutoff modes.

Notice that the theoretical curves for B2 and B3 both overpredict the data in Figure 6, while for B1 the theory underpredicts the data. It is this B1 liner result which initiated the near cutoff contour broadening study reported in the Appendix. Before this modification the theory underpredicted the data considerably more than in Figure 6. The equations in the Appendix represent all of the contour broadening which can be theoretically justified. Additional broadening could be empirically inserted, but this does not seem to be justified at this point in time. Other theoretically treatable effects such as modal scattering should be studied first.

The variation of attenuation directivity with liner resistance is shown in Figure 7. The agreement between theory and data is qualitatively correct but a greater sensitivity to resistance is exhibited by the theory than by the data. The agreement for the two higher resistance liners (B3 and B5) could be improved by using an empirical multiplier but then the lower resistance data would be somewhat underpredicted.

The attenuation directivity obtained from the progressive untaping of liner U1 is shown in Figure 8. For the first $L/D = 1/4$ the liner is seen to be quite effective with the theory somewhat underpredicting the peak. The theory shows very little change for the second $L/D = 1/4$ while the data shows a considerable drop in liner effectiveness. The final $L/D = 1/2$

of liner taping shows a comparison between theory and data more like the higher attenuation curves of previous figures, with the theory somewhat overpredicting the data.

An attempt was also made to predict the attenuation directivity of multiple pure tones at takeoff engine speed. Problems are immediately apparent, as illustrated in the narrow-band far-field directivity in Figure 9 for the twelfth shaft harmonic. The only simple assumption to make as to the modal content of this noise is that it exists as a 12-lobe pattern ($m = 12$). The theoretical directivity of the 12-lobe mode, first radial, is shown on the figure and the agreement looks plausible for high angles. However, the noise evident between 10 and 40 degrees indicates the presence of one or more other modes which are not so easily deduced. The sound attenuation obtained experimentally with a liner designed to remove multiple pure tones (ref. 7) reached about 18 decibels for a liner length of $L/D = 1/4$. However, the theoretical attenuation using equal acoustic power per mode (which is not considered a good assumption for MPTs) reached only about 5 decibels. With the assumption that only the $m = 12$ mode is present, the theoretical attenuation is also only about 5 decibels. It is obvious that in its present form, this method cannot be used for multiple pure tones where only one or a few modes are dominant. It is clear that modal scattering plays an important role here, and the following example emphasizes this point. The 12-lobe pattern has $\xi = 1.042$ in the hard-wall duct. At the liner optimum impedance for this mode, the lowest radial order has $\xi = 0.807$ with an attenuation of 2.2 times that predicted by equation (2). The higher radial modes, while not investigated, may have even higher attenuation. Thus, it is seen that modal scattering must be incorporated into this program if it is to be used for multiple pure tones. Of course, exact propagation analysis can also be used in this case involving only a few incident modes.

CONCLUDING REMARKS

This paper has presented the initial comparison between experimental suppression directivity data and the theoretical predictions using the simplified liner evaluation program based upon mode cutoff ratio. It should again be pointed out that the prediction of attenuation directivity is an extremely demanding objective. This prediction involves noise source considerations, duct propagation, and far-field radiation from the duct termination. In spite of this complexity, the theoretical model provided reasonable quantitative and excellent qualitative agreement with the experimental data. The results of the theory presented here did not have any empirical corrections applied. Empirical correction is a path that will be pursued. There are many elements in this program which may be individually

corrected and tested as experimental evidence points to the need. The theoretical model can also be improved. Inclusion of modal scattering at the liner input may be of benefit. This has been shown to be essential for possible single mode propagation such as multiple pure tones. The addition of an unflanged duct radiation model will also provide an improvement. Also, the potential changes in the radiation pattern due to modal scattering through duct area changes such as the throat and the inlet lip must be investigated. Several of the above suggested additions to the theory, as well as a more careful evaluation of the source power distribution, may provide a better agreement between theoretical and experimental far-field directivity attenuation.

APPENDIX - OFF OPTIMUM ATTENUATION

The method for calculating liner attenuation used in this report does not involve exact modal propagation calculations, but instead is based upon correlations derived from these calculations. The correlations involve the values of the maximum possible attenuation ($\Delta dB_m/L/D$) as expressed in equation (2) in the text and of the optimum impedance components (θ_m, X_m) based upon the equations in reference 4. Since in general the impedance of interest in a calculation is not the optimum impedance, a method must be provided to calculate attenuation at any arbitrary impedance. Such a method was previously reported in reference 10, which provided constant damping circular contours in the impedance plane to approximate the exact contours. An example of these circular contours was shown in Figure 1. This correlation was based upon well propagating modes (large ξ) and did not consider the effects of a boundary layer near the wall.

Comparisons of theoretical and experimental far-field attenuation directivities as presented in this paper indicated that the correlation did not provide sufficiently broad attenuation contours for modes near cutoff. A closer examination of the exact attenuation contours for modes near cutoff showed that this was indeed the case. Also discovered in this reexamination of exact theory is that for well propagating modes, when the boundary layer caused a large reduction of optimum resistance (see ref. 4), the entire system of attenuation contours was compressed.

The new correlation, an example of which is shown in Figure 2, accounts for near cutoff broadening and compression due to the boundary layer. The basic equation for the circular contours is,

$$(\theta - \theta_c)^2 + (\chi - \chi_c)^2 = \mathcal{R}^2 \tag{A1}$$

where the coordinates for the center of the circle are,

$$\theta_c = \theta_m + \frac{F\gamma^2(\gamma-1)(\xi^4+2.1)}{(\gamma^2+7)\quad \xi^4}\left(\frac{\theta_m}{\theta_{mo}}\right) \tag{A2}$$

and

$$\chi_c = \chi_m \tag{A3}$$

The radius of the circular contour is,

$$\mathcal{R} = \frac{\Theta_m(\gamma-1)^2}{\gamma(\gamma+0.7)} + \frac{F\gamma^2(\gamma-1)(\xi^4+2.1)}{(\gamma^2+7)\quad \xi^4}\left(\frac{\Theta_m}{\Theta_{mo}}\right) \tag{A4}$$

where

$$F = \frac{8.7}{\frac{\Delta dBm}{L/D}\ (1+M_D)^2} \tag{A5}$$

and

$$\gamma = \frac{\Delta dBm}{\Delta dB} \tag{A6}$$

which is the ratio of maximum possible attenuation to the actual attenuation on the contour.

The quantity θ_m/θ_{mo} represents the effect of contour compression due to boundary layer refraction. The optimum resistance with a boundary layer (θ_m), without a boundary layer (θ_{mo}) and the optimum reactance (X_m) are all found using the correlations of reference 4. Equation (2) in the text provides the value of $\Delta dB_m/L/D$.

Equations (A2), (A3), and (A4) can be used to construct the circular contour system as illustrated in Figure 2. In the actual attenuation program used in this paper, equation (A1), using equations (A3), (A4), and (A5), was solved by iteration to find the attenuation at any arbitrary impedance. All quantities in the equations are known except ΔdB in equation (A6) for γ. To start the iteration γ is set equal to one and then increased until equation (A1) is satisfied. With γ thus determined, the desired attenuation (ΔdB) at the arbitrary impedance is found from equation (A6).

REFERENCES

1. Motsinger, R. E., Kraft, R. E., and Zwick, J. W., "Design of Optimum Acoustic Treatment for Rectangular Ducts with Flow," ASME Paper 76 GT-113, Mar. 1976.

2. Minner, G. L., and Rice, E. J., "Computer Method for Design of Acoustic Liners for Turbofan Engines," NASA TMX-3317, 1976.

3. Rice, E. J., "Inlet Noise Suppressor Design Method Based Upon the Distribution of Acoustic Power with Mode Cutoff Ratio," Advances in Engineering Science, Vol. 3, NASA CP-2001, 1976, pp. 883-894.

4. Rice, E. J., "Optimum Wall Impedance for Spinning Modes - A Correlation with Mode Cutoff Ratio," Journal of Aircraft, Vol. 16, May 1979, pp. 336-343.

5. Rice, E. J., "Multimodal Far-Field Acoustic Radiation Pattern Using Mode Cutoff Ratio," AIAA Journal, Vol. 16, Sept. 1978, pp. 906-911.

6. Rice, E. J., "Modal Density Function and Number of Propagating Modes in Ducts," NASA TMX-73539, 1976.

7. Heidelberg, L. J., Rice, E. J., and Homyak, L., "Experimental Evaluation of a Spinning Mode Acoustic Treatment Design Concept for Aircraft Inlets," NASA TP-1613, 1980.

8. Rice, E. J., "Acoustic Liner Optimum Impedance for Spinning Modes with Mode Cutoff Ratio as the Design Criterion," AIAA Paper 76-516, July 1976; also NASA TMX-73411, 1976.

9. Rice, E. J., "Spinning Mode Sound Propagation in Ducts with Acoustic Treatment and Sheared Flow," in Aeroacoustics: Fan Noise and Control; Duct Acoustics; Rotor Noise, edited by I. R. Schwartz, H. T. Nagamatsu, and W. C. Straehle, AIAA Progress in Astronautics and Astronautics, Vol. 44, AIAA, New York, 1976, pp. 475-505 (also AIAA Paper 75-519, Mar. 1975 and NASA TM-X-71672, 1975).

10. Rice, E. J., "Attenuation of Sound in Ducts with Acoustic Treatment: A Generalized Approximate Equation," NASA TMX-71830, 1975.

11. Saule, A. V., "Modal Structure Inferred from Static Far-Field Noise Directivity," AIAA Paper No. 76-574, July 1976; also NASA TMX-71909, 1976.

12. Saule, A. V., and Rice, E. J., "Far-Field Multimodal Acoustic Radiation Directivity," NASA TM-73839, 1977.

13. Rice, E. J., Heidmann, M. F., and Sofrin, T. G., "Modal Propagation Angles in a Cylindrical Duct with Flow and Their Relation to Sound Radiation," AIAA Paper No. 79-0183, Jan. 1979; also NASA TM-79030, 1978.

14. Heidmann, M. F., Saule, A. V., and McArdle, J. G., "Analysis of Radiation Patterns of Interaction Tones Generated by Inlet Rods in the JT15D Engine," AIAA Paper 79-0581, Mar. 1979; also NASA TM-79074, 1979.

15. Lansing, D. L., Drischler, J. A., and Pusey, C. G., "Radiation of Sound from an Unflanged Circular Duct with Flow," Acoustical Society 79th Spring Meeting, Atlantic City, N.J., April 21-24, 1970.

16. Homicz, G. F., and Lordi, J. A., "A Note on the Radiative Directivity Patterns of Duct Acoustic Modes," Journal of Sound and Vibration, Vol. 41, Aug. 8, 1975, pp. 283-290.

17. Savkar, S. D., "Radiation of Cylindrical Duct Acoustic Modes with Flow Mismatch," Journal of Sound and Vibration, Vol. 42, Oct. 8, 1975, pp. 363-386.

18. Rice, E. J., "Spinning Mode Sound Propagation in Ducts with Acoustic Treatment," NASA TN D-7913, 1975.

19. Motzinger, R. E., Kraft, R. E., Zwick, J. W., Vukelich, S. I., Miner, G. L., and Baumeister, K. J., "Optimization of Suppression for Two-Element Treatment Liners for Turbomachinery Exhaust Ducts," General Electric Co., Cincinnati, Ohio, R76AEG256, April 1976 (NASA CR-134997).

20. Pickett, G. F., Sofrin, T. G., and Wells, R. A., "Method of Fan Sound Mode Structure Determination," Pratt and Whitney Aircraft, East Hartford, Conn., PWA-5554-3, Aug. 1977. (NASA-CR-135293).

21. Rice, E. J., "Modal Propagation Angles in Ducts with Soft Walls and Their Connection with Suppressor Performance," AIAA Paper No. 79-0624, Mar. 1979; also NASA TM-79081, 1979.

Table I. - Design Parameters for Acoustic Liner Panels

Liner	Open area ratio σ, percent	Backing depth, b cm	(inches)
B1	5.3	0.193	(0.076)
B2	3.8	0.328	(0.129)
B3	5.3	0.531	(0.209)
B4	11.2	0.688	(0.271)
B5	3.8	0.475	(0.180)
U1	5.3	0.363	(0.143)

Facing sheet thickness t, 0.051 cm (0.020 in) thick
Orifice diameter d_o, 0.140 cm (0.055 in) diameter
All sections L/D = 1/2

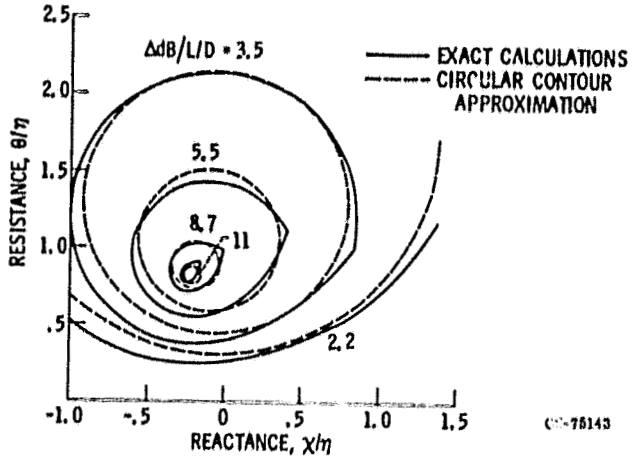

Figure 1. - Comparison of exact and approximate equal damping contours for a well propagating mode (ref. 10). m = 7, $\mu = 1$, $\eta = 10$, $M_D = -0.4$, $\epsilon = 0.002$

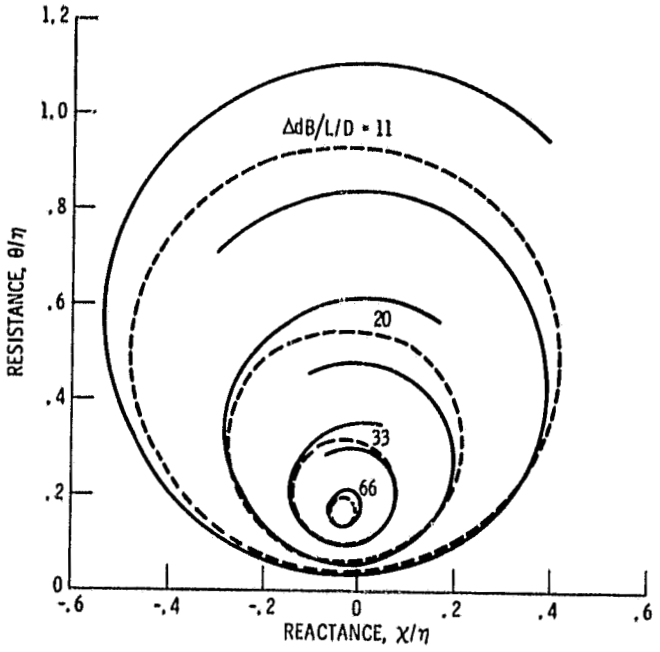

Figure 2. - Comparison of exact and approximate equal damping contours for a near cutoff mode. m = 29, $\mu = 3$, $\xi = 1.0626$, $\eta = 14.2$, $M_D = -0.38$, $\epsilon = 0.001$.

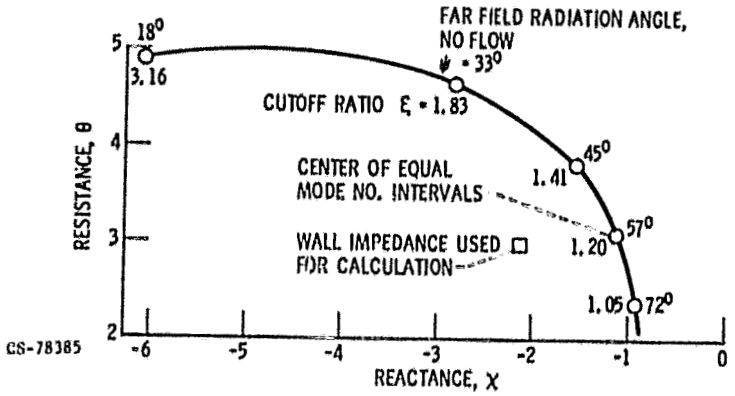

Figure 3. - Optimum impedance locus with equal mode number intervals.

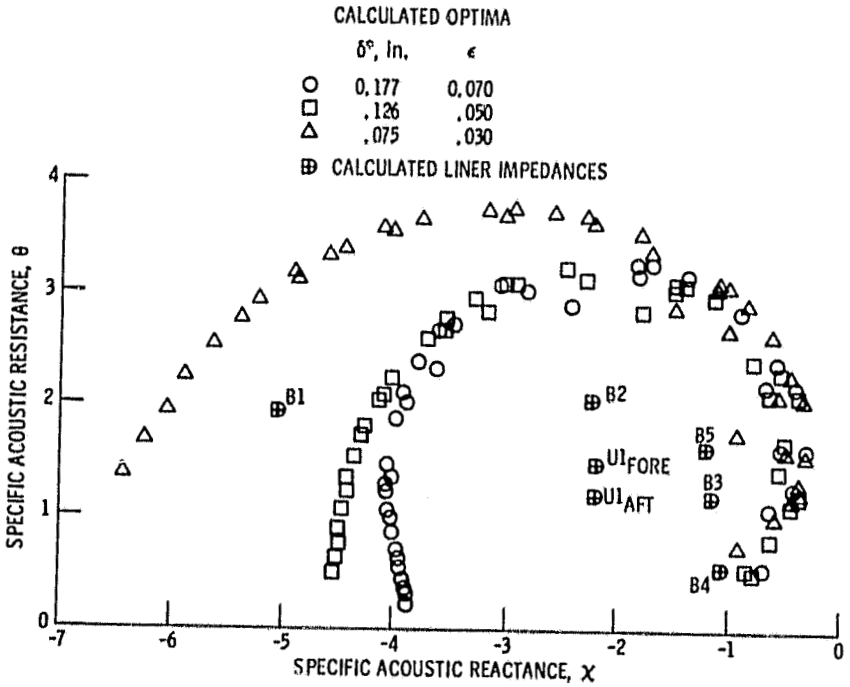

Figure 4. - Calculated optimum impedance loci and wall impedances for three suppressors. f = 4734 Hz, η = 14.2, M_D = -0.38, D = 40.3 in.

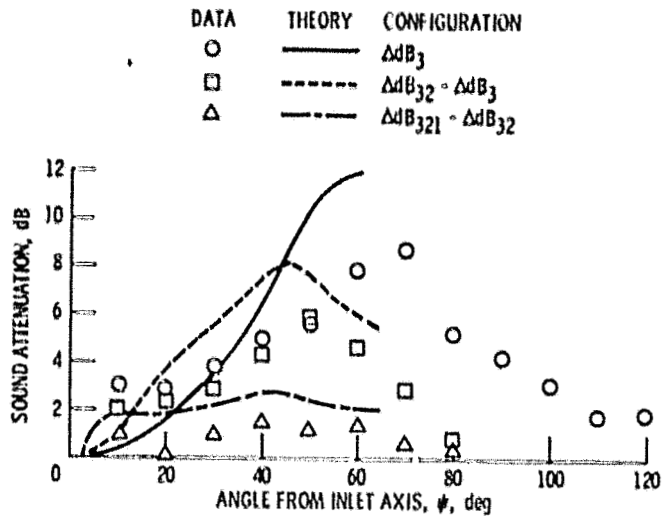

Figure 5. - Incremental experimental and theoretical directivity attenuations for liners B1, B2, and B3. $\eta = 14.2$, M_{jj} -0.38, f = 4734 Hz

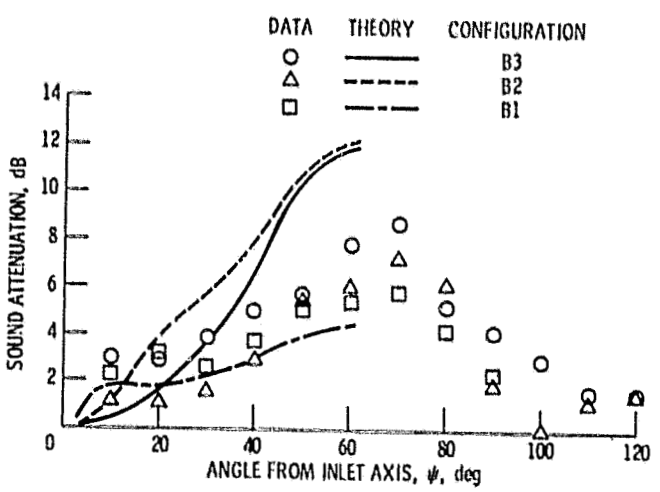

Figure 6. - Attenuation directivity for isolated tests of liners B1, B2, and B3. $\eta = 14.2$, $M_D = -0.38$, f = 4734 Hz

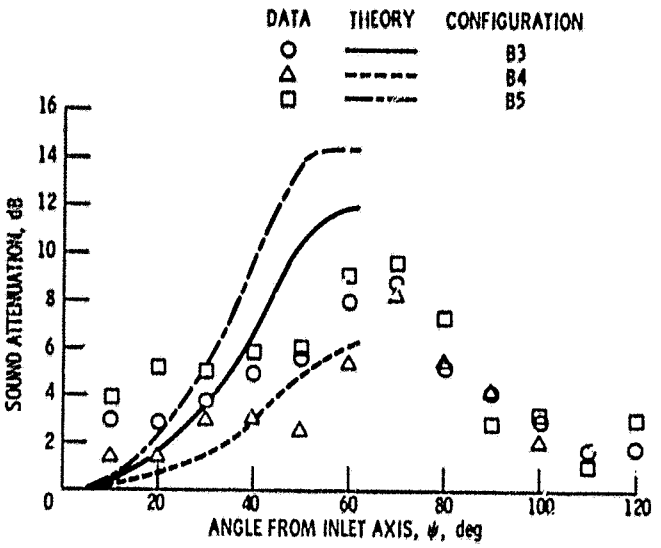

Figure 7. - Attenuation directivity for liners with varying resistance, $\eta = 14.2$, $M_D = -0.38$, $f = 4734$ Hz

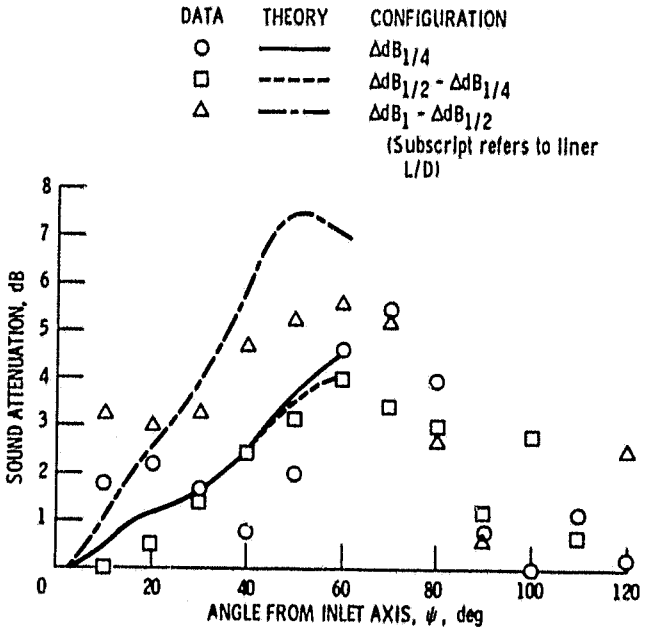

Figure 8. - Incremental experimental and theoretical directivity attenuations for uniform liner U1. $\eta = 14.2$, $M_D = -0.38$, $f = 4734$ Hz

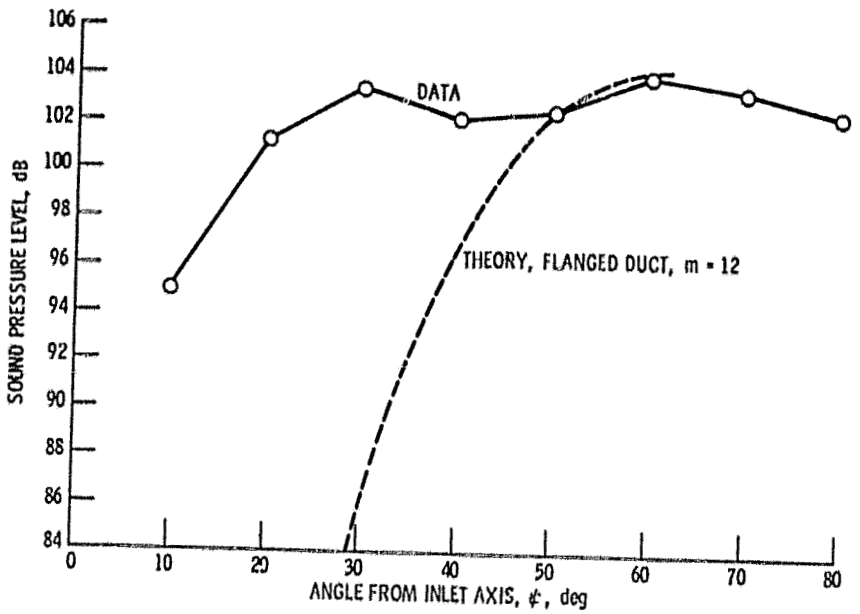

Figure 9. - Narrow band far-field directivity for the twelfth harmonic of shaft rotational frequency. f = 1420 Hz, M_D = -0.38.